Predictions of Thermo-Mechanical Properties of Cross-Linked Polyacrylamide Hydrogels Using Molecular Simulations

Meng An, Baris Demir, Xiao Wan, Han Meng, Nuo Yang, and Tiffany R. Walsh**

Hydrophilic acrylamide-based hydrogels are emerging platforms for numerous applications, but the resources to fully exploit these materials are currently limited. A deep understanding of the molecular-level structure/property relationships in hydrogels is crucial to progressing these efforts. Such relationships can be challenging to elucidate on the basis of experimental data alone. Here, molecular simulations are used as a complementary strategy to reveal the molecular-level phenomena that govern the thermo-mechanical properties of hydrogels. The focus is on acrylamide-based hydrogels cross-linked with *N*,*N*′-methylenebisacrylamide, generated using previously established computational cross-linking procedure. The water content is found to be a key determinant in the elastic response of these hydrogels, with enhanced tensile and shear properties at low water content. However, it is also found that increasing water content enhances the hydrogel's thermal conductivity, with the dominant contribution arising from the non-bonded contributions to the heat flux. In addition, chemical cross-linking improves the heat transfer properties of the hydrogel, whereas a reduction in convective heat transfer is predicted with an increase in hydrogel cross-linking. These simulations provide a rational basis for designing and testing customized hydrogel formulations for maximizing both thermal conductivity and mechanical properties.

1. Introduction

Hydrogels are water-containing, hydrophilic polymer networks that are found ubiquitously in nature in the form of hydrated biological tissues.[1] The properties of these materials are conferred by a variety of mechanisms spanning physical entanglement of polymer chains, electrostatic interactions, and covalent-bond cross-linking.[2] Owing to their unique characteristics of flexibility and biocompatibility, hydrogels are ideal for use in applications such as tissue engineering,[3,4] drug delivery,[5–7] desalination,[8] soft electronics,[9–11] and for technologies that include human–machine interfaces and soft robotics.[12,13] However, the full potential of hydrogel applications is often limited by their mechanical and thermal properties.[14]

Over the past decades, experimental studies into the mechanical strength of hydrogels have enhanced our understanding of the structure/property relationships of tough hydrogels.[1,15,16] Zhao summarized the various mechanisms for designing tough hydrogels and generally noted that tough hydrogels could dissipate energy and maintain high elasticity.[16,17] In a related study, Gong et al. reported a double-network hydrogel structure formed by two inter-penetrating hydrophilic polymer networks, which featured extraordinary mechanical properties due to the effective dissipation of mechanical stress.[18,19] In recent studies, Suo et al. developed novel ionically and chemically cross-linked poly(acrylamide) (PAAm) hydrogels with good stretchability, plastic deformability, and autonomous self-healability.[15,20]

In contrast to the large number of published studies focused on the mechanical properties of hydrogels, reported investigations of the thermal properties of hydrogels[21–24] are relatively fewer in number. For instance, Tang et al.[21] reported the thermal conductivity of pure PAAm and chemically cross-linked PAAm with *N*-methylenebisacrylamide (MBAm), measured using the 3ω technique, as a function of water content. In this technique, an electrical current is applied to a heater that is in physical contact with the hydrogel sample, and the thermal conductivity is then inferred by relating the thermal oscillations to amplitude of the power per unit length generated by the current passing

Dr. M. An, X. Wan, H. Meng, Prof. N. Yang
State Key Laboratory of Coal Combustion
Huazhong University of Science and Technology
Wuhan 430074, P. R. China
E-mail: nuo@hust.edu.cn
Dr. M. An
College of Mechanical and Electrical Engineering
Shaanxi University of Science and Technology
6 Xuefuzhong Road, Weiyangdaxueyuan, Xi'an 710021, P. R. China
Dr. B. Demir, Prof. T. R. Walsh
Institute for Frontier Materials
Deakin University
Geelong, VIC 3216, Australia
E-mail: tiffany.walsh@deakin.edu.au
X. Wan, H. Meng, Prof. N. Yang
Nano Interface Center for Energy
School of Energy and Power Engineering
Huazhong University of Science and Technology
Wuhan 430074, P. R. China

The ORCID identification number(s) for the author(s) of this article can be found under https://doi.org/10.1002/adts.201800153

DOI: 10.1002/adts.201800153

through the heater.[25] These authors reported an experimental thermal conductivity of pure PAAm hydrogel (with water content) of 0.33 $W m^{-1} K^{-1}$ and found that cross-linking with MBAm improved the thermal conductivity by 54%. Enhancements in the thermal conductivity of hydrogels might be attributed to the formation of chemical cross-link bonds between the polymer chains of the hydrogels. Overall, chemical cross-linking in hydrogels has the potential to deliver substantially improved toughness via spatiotemporal precision, in addition to conferring enhanced thermal properties.

Experimental elucidation of structure/property relationships for such cross-linked hydrogels can often be challenging to accomplish due to several reasons, including the resolution of the experimental technique (i.e., low resolution can limit the analysis of the cross-linked hydrogels owing to the hydrogel network's inability to dissolve).[26,27] To address this challenge, computational techniques such as molecular dynamics (MD) simulations can complement experimental efforts and provide critical insights at the atomistic level into new, knowledge-based strategies for designing and testing hydrogels. Several MD simulation studies of hydrogels have been previously reported in the literature. Most of these reports focused on molecular-level structuring and diffusion in hydrogels,[28–34] with a small number of these reports devoted to probing hydrogel mechanical response under tensile deformation.[35–38] In one of the early MD simulation studies, Tamai et al.[28] investigated the effect of water content on the water–polymer interactions in three hydrogels: poly(vinyl alcohol) (PVA), poly(vinyl methyl ether) (PVME), and poly(*N*-isopropylacrylamide (PNiPAM). These authors analyzed hydrogen-bonding distributions as a function of water content and temperature, to obtain a trend in the hydrophilic character of these three hydrogels. Unfortunately, the periodic cell dimensions used in this work (ranging between 19.6 and 26.3 Å) were very small relative to the inherent length-scales of the constituent molecules. This scenario may have led to unphysical interactions between the polymer chains in the simulation cell. A similar study reported by Netz and Dorfmüller[29] predicted the diffusion of water molecules in PAAm–MBAm hydrogels, with various system sizes (periodic cell dimensions of 23.5 and 32 Å). However, the short MD simulation times used for the calculation of diffusion coefficients (around 70 ps), which were laudable for their time, might not have provided an unbiased evaluation of this property.

In addition to investigations of the molecular-level organization of hydrogels, the mechanical response of these materials has also been studied using molecular simulations. However, the number of such studies in the literature is limited. For instance, Jang et al.[35] predicted the mechanical response of three hydrogels, comprising poly(ethylene oxide) (PEO), poly(acrylic acid) (PAA), and the double network of PEO–PAA, under tensile deformation. These authors predicted that at very high deformation, for example, 200% tensile strain, the mechanical response of the double-network PEO–PAA hydrogel was relatively greater than those estimated for PEO and PAA. However, at such large strains, this result might be ascribed to an inherent limitation of the force field used in this work, in which bond breakage/formation could not be captured *on-the-fly*. This limitation might have therefore caused unphysically long bond extensions at high strain values, which in turn can confer unphysically high stresses in the hydrogel. In another study, Lee et al.[36] computationally probed the influence of water content on the elastic modulus of poly(*N*-vinyl-2-pyrrolidone-*co*-2-hydroxyethyl methacrylate) hydrogels. These authors reported that water loading detrimentally affected the elastic modulus, but did not provide a molecular-level explanation for this finding.

In earlier MD simulation studies where the hydrogel polymer chains were chemically cross-linked with cross-linker molecules,[29,30,33,34,39] the computational cross-linking protocol was typically not reported in sufficient detail to allow reproduction of the reported results. Moreover, in most of these studies, the cross-links were typically formed out of the simulation cell (i.e., as free-standing dendrimer-like structures, with complete cross-link conversion) and were not formed *on-the-fly* during the simulation. For instance, Wu et al.[27] computationally investigated the diffusion of water and ions in poly(ethylene glycol) (PEG) hydrogels following this "dendrimer-based" procedure. However, this sample preparation procedure cannot capture all of the relevant properties of the system (such as the mechanical properties) as a function of the degree of cross-linking (DOC), which can play an important role in determining the ultimate properties of the hydrogel.[27] Ideally, the gradual formation of new cross-link bonds between the polymer and the cross-linker should be captured as the MD simulation proceeds, to allow hydrogel samples with different DOC values to be prepared and analyzed. In a recent study, a hydrogel composed of acrylamide (AAm) monomers and MBAm molecules was modeled and subjected to thermal conductivity calculations.[39] Unfortunately, the lack of details of sample preparation procedure (e.g., the cross-linking protocol) reported in ref. [39] made the reproducibility of these reported results challenging.

Despite the significant number of MD simulation studies reported on the structural investigation of hydrogels, there are very few MD simulation studies reported in the literature regarding the prediction of *cross-linked* hydrogel thermal conductivities[37] or even *un-crosslinked* mixtures of PAAm and MBAm molecules, in the absence of water.[21] Therefore, our findings presented herein will bridge three critical gaps in the modeling of the hydrogels using all-atom MD simulations. First, we introduce a robust and reproducible dynamic cross-linking protocol to computationally generate cross-linked PAAm–MBAm hydrogel samples. This preparation procedure allows us to capture the thermo-mechanical properties of these hydrogels as a function of the DOC, based on our previous work on epoxy resins.[40–43] Second, we predict the tensile and shear response of these PAAm–MBAm hydrogel samples as a function of the DOC and water content, using non-equilibrium MD (NEMD) simulations. Third, we predict the thermal conductivities of these hydrogels as a function of a range of factors including the water content and the DOC, via equilibrium MD (EMD) simulations.

We have focused here on PAAm hydrogels cross-linked with MBAm because these materials have been the subject of numerous previous experimental investigations and, as a result, a range of experimental results for these hydrogels are available.[44–47] This allows us to validate our approach via comparison of our computationally predicted mechanical properties with relevant experimental findings. Unfortunately, the comparison of our predicted thermal conductivities with experimental values was hampered by a scarcity of relevant experimental data. Moreover, we

have used our MD simulations to probe the influence of several parameters relevant to the hydrogel properties, including the simulation cell size, the oligomer chain length of PAAm, the DOC, and the water content.

2. Experimental Section

2.1. General Simulation Details

All-atom molecular dynamics simulations were performed using the OPLS force field (FF)[48] for the PAAm and MBAm molecules and the TIP4P water model.[49,50] Full details of all FF parameters and the labels for unique atomic sites are provided in Tables S1–S4 and Figure S1, Supporting Information, respectively. The water molecules were kept rigid via the SHAKE algorithm[51] throughout the simulations. The system temperature and pressure were controlled via the Nose–Hoover thermostat[52] and barostat,[53,54] respectively. The long-range van der Waals (vdW) and Coulombic interactions were cut off at an interatomic distance of 12 Å. The long-ranged contribution to the electrostatic interactions was calculated via the particle–particle–particle–mesh (PPPM) algorithm.[55] A time-step of 1 fs was used in the simulations, except for the thermal conductivity calculations, where a time-step of 0.1 fs was used. Periodic boundary conditions were implemented in all three principal directions. All simulations were performed using the LAMMPS software package (https://lammps.sandia.gov).[56]

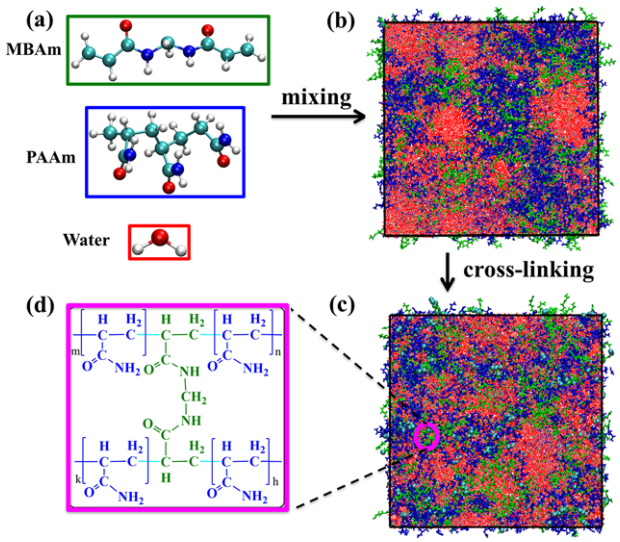

Figure 1. Overview of our computational hydrogel sample preparation. a) Molecular structures of pre-polymerized PAAm oligomer (for illustrative purposes only, depicted here with 3 AAm repeat units), MBAm, and water molecules. (Carbon, nitrogen, oxygen and hydrogen atoms are in cyan, blue, red and white, respectively.) b) A simulation cell comprising an uncrosslinked liquid mixture of water (red), MBAm molecules (green), and pre-polymerized PAAm oligomers (blue). c) A simulation cell comprising a cross-linked hydrogel sample (spheres in cyan indicate the chemically reacted atomic sites). d) Molecular structures of the pre-polymerized PAAm oligomers (in blue) covalently cross-linked with the MBAm molecules (in green). The subscripts (m, n, k, and h) denote the length of PAAm oligomer in terms of the number of AAm repeat units. In this work, these subscripts are set to $m = n = k = h$. In (b) and (c), the black solid lines indicate the periodic cell boundaries.

2.2. Sample Preparation Details

The hydrogel systems comprised different relative proportions of water, MBAm monomers, and pre-polymerized PAAm oligomeric chains (**Figure 1**a). Hydrogel systems with 10, 50, and 90 wt% of water were considered. Samples with different values of the DOC were also prepared, specifically with DOC values of 25%, 50%, and 85%. Here, the DOC is defined to be the ratio between the number of reacted PAAm oligomer reactive atomic sites and the total number of all PAAm oligomer reactive atomic sites present in the simulation system. For example, each PAAm oligomer has two reactive atomic sites per chain end (i.e., a total of four reactive sites per oligomer chain). Therefore, a fully cross-linked (i.e., DOC of 100%) system that initially contained 10 PAAm oligomers would yield a theoretical maximum of a total of 40 new cross-link bonds.

In addition to these two system specifications (i.e., the water content and DOC), pre-polymerized oligomers of PAAm with different chain lengths in the hydrogel samples, ranging from 10 to 32 AAm repeat units, were also used. To be clear, by definition, a hydrogel sample with a DOC of 0% (i.e., the uncrosslinked hydrogel) does not correspond to a sample containing unreacted AAm monomers and MBAm cross-linkers, but rather corresponds to a sample in which the pre-polymerized PAAm oligomers and MBAm cross-linkers have not yet reacted. In this sense, even the "0% DOC" system is partially polymerized due to the presence of the pre-polymerized PAAm oligomers. In the current work, the dynamic formation of PAAm oligomers was not modeled via the radical polymerization of the AAm repeat units. This type of modeling presents unique technical challenges that will be addressed in a future study. Therefore, by definition, the term "cross-linking" strictly corresponds only to the formation of new covalent bonds between the pre-polymerized PAAm oligomers and the MBAm cross-linker molecules.

The initial hydrogel samples were prepared by randomly placing the pre-polymerized PAAm oligomer chains, MBAm molecules, and water molecules together in a cubic simulation cell with a constant AAm/MBAm ratio of 4:1, which was based on the ratio of reactivity of the MBAm molecule with respect to the PAAm oligomer. The total number of AAm repeat units comprising the PAAm content was kept fixed (for a given value of the water content), but was partitioned into a differing number of PAAm oligomeric chains, depending on the chain length under consideration. For example, in the system with a water content of 50 wt%, a total of 320 AAm repeat units were used, which in one case was partitioned into 32 × 10-mer chains of PAAm along with 80 MBAm molecules, while in another case the 50 wt% system was partitioned into 20× chains of 16-mer PAAm oligomers along with 80 MBAm molecules. Similarly, there were 60× and 8 × 10-mer-long PAAm oligomer chains present in the hydrogel samples with a water content of 10 and 90 wt%, respectively. To alter the water content of the samples, the number of water molecules added to the sample was varied, with a total number of 390, 1952, and 3514 water molecules for the hydrogel samples

with a water content of 10, 50, and 90 wt%, respectively. Based on this change in the total number of water molecules in the hydrogel samples, the total number of AAm/MBAm units comprised 600/150, 320/80, and 80/20 for the hydrogel samples with a water content of 10, 50, and 90 wt%, respectively. The size of the cubic simulation cells differed, depending on the different water content, ranging between 46.1 × 46.1 × 46.1 Å and 48.9 × 48.0 × 48.9 Å. The density of the hydrogel samples ranged between 1.021 g cm^{-3} (with a water content of 90 wt% and a DOC of 0%) and 1.288 g cm^{-3} (with a water content of 10 wt% and a DOC of 85%).

The content of the hydrogel samples described above was for a sample size of 1 unit cell (uc). To explore system-size effects, four additional hydrogel samples were also generated, two with a size of 4 uc and two with a size of 8 uc, each with a water content of 50 wt%, at DOC values of 0% and 85%. The content of the polymer and water in each of these new larger samples could be obtained by multiplying the number of each type of constituent molecule in the 1-uc samples (summarized above) by 4× and 8× for the 4-uc and 8-uc samples, respectively. For instance, 128× and 256 × 10-mer chains of pre-polymerized PAAm oligomers were used in the 4-uc and 8-uc hydrogel samples, respectively. Further details regarding the system size and number of molecules in each hydrogel sample are provided in Table S5, Supporting Information.

The samples were initially generated at a low density and were subsequently subjected to geometry optimization and MD simulations. The equilibrium density of the samples at 323 K (a typical experimental reaction temperature for this hydrogel system[57]) and 1 bar were obtained using isothermal–isobaric simulations (i.e., MD simulations in the *NPT* ensemble) for 300 ps. Following this stage, further equilibration, namely a simulated annealing (SA) procedure, was carried out to ensure adequate mixing of the molecules in the simulation cell (illustrated in Figure 1b) prior to initiating the computational cross-linking process. In the SA procedure, the samples were heated and cooled between 323 and 700 K via canonical ensemble MD simulations (i.e., MD simulations in the *NVT* ensemble). The total simulation time for each SA cycle was 1.9 ns, and two SA cycles per sample were carried out. The resultant structures arising from the SA equilibration process were then used as input for the computational cross-linking procedure. In this procedure, cross-link bonds were formed *on-the-fly* between the pre-polymerized PAAm oligomers and the MBAm molecules, using an in situ dynamic cross-linking procedure previously established for epoxy resins by Demir and Walsh.[40] These new, dynamically created covalent bonds between the pre-polymerized PAAm oligomers and the MBAm molecules resulted in the formation of a 3-D polymer network, as illustrated in Figure 1c,d.

Summarized briefly, in the computational dynamic cross-linking procedure, pairs of reactive atomic sites located within an initial cut-off distance were first detected and then covalent cross-link bonds formed between the reactive atomic pairs (located at the chain ends of the PAAm oligomers and the MBAm monomers) at 323 K. The samples were relaxed via a multi-step relaxation procedure using MD simulations in the *NVT* ensemble, to relieve the potentially high internal stress arising from the initial formation of the new bonds.[40] The details for this relaxation step are provided in Table S6, Supporting Information. New pairs of reactive atomic sites were searched for within the same cut-off distance for ten times before the cut-off distance was incremented by 0.5 Å. This procedure was repeated until the target DOC was achieved. These resultant cross-linked hydrogel samples at different DOC values, water content, and system size were equilibrated at 300 K and atmospheric pressure via MD simulations in the *NPT* ensemble for 200 ps prior to the prediction of their mechanical properties and thermal conductivities. The details (e.g., the density and simulation cell size) of the hydrogel samples used to predict thermo-mechanical properties are provided in Table S7, Supporting Information, along with full details of the sample preparation procedure.

2.3. Structural Characterization

Molecular-level structuring of the hydrogel samples can provide insights into the ultimate properties of these materials. To this end, radial distribution functions (RDFs) between the different oxygen atomic sites present in the constituent molecules in the hydrogel (i.e., the oxygen atoms of the water molecules, the MBAm molecules, and the PAAm oligomers) were calculated. These RDFs were generated based on the equilibrated samples, using MD simulations in the *NVT* ensemble at 300 K for 200 ps. Specifically, focus was on a sample with a DOC of 50%, a water content of 50 wt%, and a system size of 1 uc. The basis for this choice was that this system was at the mid-range of DOC values and water content values studied here, which could reflect a representative molecular-level structuring in the hydrogel samples. The MD simulation results were then analyzed to produce the RDF plots using the *in-house* codes. To accomplish this, the frames from the trajectory of the 200 ps *NVT* MD simulation every 1 ps, corresponding to 200 frames in total, were saved and the RDF plots were averaged over these 200 frames.

A clustering analysis was also performed to probe the size of the water clusters in the hydrogel samples, which, in turn, could contribute to the total heat flux in the hydrogel. To achieve this, the *k*-means algorithm was used, which, with other clustering algorithms, was used to analyze trajectories in MD simulations.[58–62] The *k*-means algorithm is an unsupervised machine learning algorithm that uses a predefined number of initially determined centroids, *k* (i.e., the total number of clusters that is initially determined), to assign each data point (i.e., the normalized Cartesian coordinates of the water oxygen atoms) to clusters in the simulation cell. Iteratively, these *k* centroids are used to calculate the distances of each data point to these centroids, and based on the shortest distance between each data point and centroids, the data points are assigned to clusters. The new centroids are calculated as the mean of the data points in each cluster. This procedure is repeated until convergence, namely the point at which the cluster size and cluster members remained invariant to iteration cycle. To accomplish this, the scikit-learn library in Python was used.[63]

Since the *k*-means algorithm relies on the choice of the initial positions of the centroids, it is of utmost importance to choose appropriate initial centroids for obtaining convergence. To achieve this, the *k*-means++ technique, which is a targeted strategy for choosing these initial centroids, was used.[64] For obtaining local minima, the *k*-means algorithm was run 10 000

times using different centroid positions. One thousand iterations were performed for each run to ensure convergence. When the distance between successive centroids was less than the given tolerance, the process was deemed as converged. The convergence tolerance was set to 1×10^{-4} Å. The results of the run, which gave the smallest total sum of square error (SSE), were chosen as the final set of clusters. The SSE is the sum of the squared distances of all the data points within the cluster to the centroid of the same cluster and summed over all k clusters. In this analysis, three hydrogel samples with different water loadings at a DOC of 50% (i.e., at water loadings of 10, 50, and 90 wt%) were tested. Only one snapshot (the same configuration that was used as a basis for the computational mechanical testing) was analyzed for each hydrogel system.

To determine the optimal number of clusters, plots of the SSE versus the number of clusters were produced. The elbow technique[58] was used to find the optimal number of clusters. In this plot, the optimal number of clusters was determined as the point where adding more clusters does not provide new information (i.e., the point at which the SSE does not decrease appreciably with an increase in the number of clusters). Periodicity was not considered in the analysis. The k-means clustering analysis was merely performed to approximately probe how the cluster size was influenced as a function of the water loading in the hydrogel sample, to interpret the trends in the predicted thermal conductivities.

2.4. Prediction of Mechanical Properties

To reveal the influence of the hydrogel system specifications (such as DOC and water content) on the ultimate mechanical properties of the hydrogel samples, the samples were tested under tensile and shear deformations using NEMD simulations. In the tensile deformation test, a strain rate of 5×10^7 s^{-1} (which is a typical tensile strain rate implemented in MD simulations) was applied in one principal direction while keeping the other two principal directions at 1 atm and 300 K via MD simulations in the *NPT* ensemble, for a duration of 4 ns. This simulation procedure was repeated for the other two principal directions (yielding a total aggregate simulation time of 12 ns over the three principal directions for one hydrogel sample). During the tensile deformation simulations, all atoms in the simulation cells were able to move in all three principal directions. The stress–strain data from each simulation were averaged over 1000 simulation steps, and stress–strain curve (SSC) was then generated using the data averaged over the three principal directions. Young's modulus values were calculated using the SSC up to 3% (proportionality limit) of the strain data. The yield strain values were also predicted for the hydrogel samples using the 0.2% offset line.[40] In this analysis, a straight line having the slope of the Young's modulus of the sample was constructed with a shift of 0.2% of strain and the intersection point of this line with the SSC was taken as the yield point. The corresponding strain and stress values at the yield point are defined here as the yield strain and yield stress.

The other mechanical test performed was the shear deformation test, in which the simulation cell was deformed with a shear rate of 1×10^{10} s^{-1} (a typical shear strain rate implemented in MD simulations[41]) while allowing all atoms to move. The shear deformation tests were performed at 300 K using the MD simulations in the *NVT* ensemble for 0.4 ns for each principal direction (yielding a total aggregate simulation time of 1.2 ns over the three principal directions for one hydrogel sample). The shear stress–strain data were averaged over every 1000 steps at each value of shear for each MD simulation performed in each principal direction. All these data were then averaged to obtain the shear SSC.

2.5. Prediction of Thermal Conductivity of Hydrogels

The thermal conductivity of the hydrogel samples was calculated using EMD simulations[65–67] based on the Green–Kubo formula using Equation (1).

$$\kappa = \frac{1}{3k_B T^2 V} = \int_0^\infty \left\langle \vec{J}(\tau) \cdot \vec{J}(0) \right\rangle dt \tag{1}$$

where κ is the thermal conductivity, k_B is the Boltzmann constant, and V and T are the volume and temperature of the simulation cell, respectively. $\vec{J}(\tau) \cdot \vec{J}(0)$ is the heat current autocorrection function, where τ is the correlation time. The angular bracket denotes an ensemble average. The heat current was calculated using Equation (2).

$$\vec{J}(\tau) = \sum_i \overrightarrow{v_i} \varepsilon_i + \frac{1}{2} \sum_{i,j\, i \neq j} \vec{r}_{ij} \left(\vec{F}_{ij} \cdot \vec{v}_i \right) \tag{2}$$

where $\overrightarrow{v_i}$ and ε_i are the velocity vector and energy (kinetic and potential) of particle i, respectively. $\vec{r}_{ij}$ and $\vec{F}_{ij}$ are the inter-particle separation vector and force vector between particle i and j, respectively.

NEMD simulations were also implemented to investigate the influence of each individual potential energy contribution (such as the non-bonded and bonded interaction terms) on the resulting predicted heat flux. The details of NEMD setup can be found in previous studies.[68,69] Based on classical statistical mechanics, Irving and Kirkwood[70] first derived the equation of energy transport in molecules in the 1950s. The equation was modified by Torii et al.[71] and was used to calculate the inter- and intra-chain energy transport with many-body potentials.[71–73] Similarly, in the LAMMPS software package,[56] the total heat flux could be decomposed into heat flux contributions from all different types of forces and a convection term using Equation (3).

$$\vec{J}_{\text{total}} = \vec{J}_{\text{total}} + \vec{J}_{\text{bond}} + \vec{J}_{\text{angle}} + \vec{J}_{\text{dihedral}} + \vec{J}_{\text{non-bonding}} \tag{3}$$

where $\vec{J}_{\text{total}}$ is the total heat flux, and the right side of Equation (3) has the contribution terms that can be calculated by Equation (4)

$$\vec{J}_{\text{total}} = \frac{1}{V} \left[\sum_i e_i \vec{v}_i - \sum_i S_i \vec{v}_i \right] \tag{4}$$

where i indicates atom i and e_i is the internal energy of atom i. S_i is the stress tensor on particle i, which is calculated using

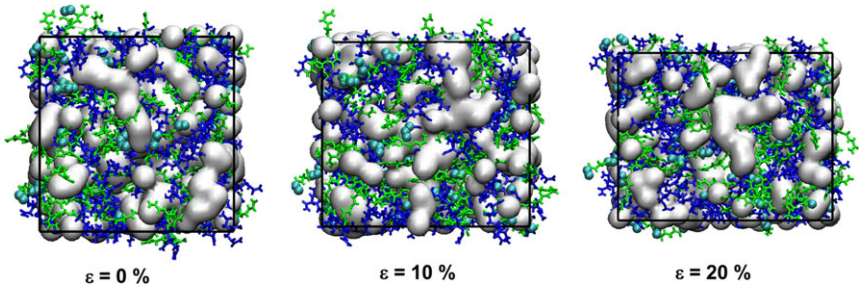

Figure 2. Snapshots of the hydrogel sample with a sample size of 1 uc with water content of 10 wt% at a DOC of 85% under tensile deformation. ε is the tensile strain. Color scheme: blue, green, cyan are for PAAm oligomers, MBAm cross-linker molecules, and chemically cross-linked atoms, respectively. The white surface represents the water molecules in the hydrogel sample. The black solid line represents the simulation cell boundaries.

Equation (5)

$$S_{ab} = -[m\vec{v}_a\vec{v}_b + \frac{1}{2}\sum_{n=1}^{N_p}\left(\vec{r}_{1a}\vec{F}_{1b} + \vec{r}_{2a}\vec{F}_{2b}\right) + \frac{1}{2}\sum_{n=1}^{N_b}\left(\vec{r}_{1a}\vec{F}_{1b} + \vec{r}_{2a}\vec{F}_{2b}\right) + \frac{1}{3}\sum_{n=1}^{N_a}\left(\vec{r}_{1a}\vec{F}_{1b} + \vec{r}_{2a}\vec{F}_{2b} + \vec{r}_{3a}\vec{F}_{3b}\right) + \frac{1}{4}\sum_{n=1}^{N_d}\left(\vec{r}_{1a}\vec{F}_{1b} + \vec{r}_{2a}\vec{F}_{2b} + \vec{r}_{3a}\vec{F}_{3b} + \vec{r}_{4a}\vec{F}_{4b}\right) \quad (5)$$

where S_{ab} is the ab component of the stress tensor on atom i, where a and b represent x, y, or z in Cartesian coordinates. $\vec{r}_1$, $\vec{r}_2$, $\vec{r}_3$, and $\vec{r}_4$ are the positions of the interacting atoms labeled 1, 2, 3, and 4; $\vec{F}_1$, $\vec{F}_2$, $\vec{F}_3$ and $\vec{F}_4$ are the force on these atoms; and N_p, N_b, N_a, and N_d are the number of non-bonding (vdW and Coulombic), bonding, angle, and dihedral interactions, respectively.

Finally, simulations on a pure water sample were also performed to provide comparisons with both thermal conductivity and coordination number data. In these simulations, 280 water molecules were placed in a cubic simulation cell with a density of 1.0 g cm^{-3}. Periodic boundary conditions were applied along the three principal directions. This system was first equilibrated for 50 ps in the *NVT* ensemble by using Nose–Hoover barostats and thermostats at a temperature of 300 K. This was followed by an MD simulation using the *NPT* (isobaric-isothermal) ensemble for 100 ps at a pressure of 1 bar and a temperature of 300 K. The obtained density of pure water system was 0.98 ± 0.03 g cm^{-3}. For the thermal conductivity simulations, the system was switched to the microcanonical (*NVE*) ensemble for a simulation of 200 ps. The size of the cubic simulation cell for pure water system was 40.6 × 40.6 × 40.6 Å.

3. Results and Discussion

3.1. Computational Mechanical Testing

Our computational mechanical tests were based on samples generated using the 10-mer pre-polymerized PAAm oligomers. The hydrogel samples were subjected to strain in each principal direction with a constant tensile strain rate, and consequently the shape of the simulation cell changed as a response to the externally applied strain. **Figure 2** shows representative snapshots of a hydrogel sample under tensile deformation at different deformation states.

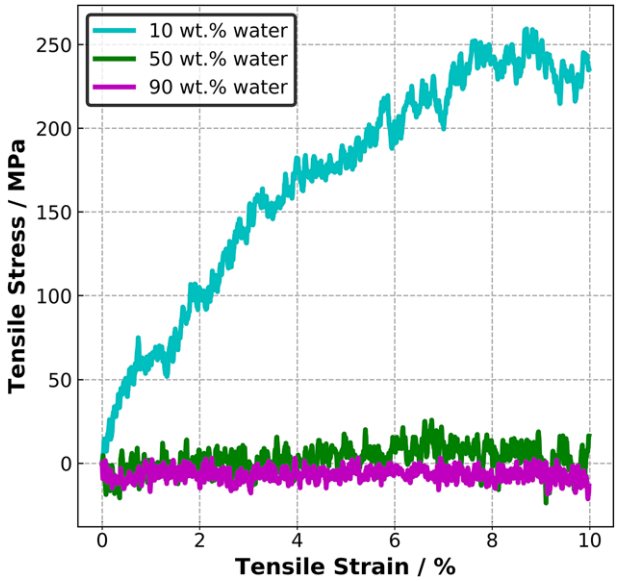

Figure 3. Predicted tensile stress versus tensile strain data for hydrogel samples (system size of 1 uc, details given in Section 2), with different water contents and a degree of cross-linking of 85%.

We first explored whether the hydrogel samples with different water content showed appreciable elastic behavior at the greatest DOC value studied here (DOC of 85%). These tensile test results (obtained using a sample size of 1 uc) are provided in **Figure 3**. These data suggest that the hydrogel samples with a water content of 50 and 90 wt% supported modest elastic properties compared to the sample with a water content of 10 wt%. This finding can be ascribed to the liquid-like state of these high water-content samples[1] under tensile deformation. Lee et al.[37] reported a similar trend for hydrogel samples of poly(*N*-vinyl-2-pyrrolidone-*co*-2-hydroxyethyl methacrylate) in their modeling study. These authors computationally tested hydrogel samples with a water content of 0 and 10 wt% and noted a decrease in the elastic modulus with an increase in the water content. Our results suggest that

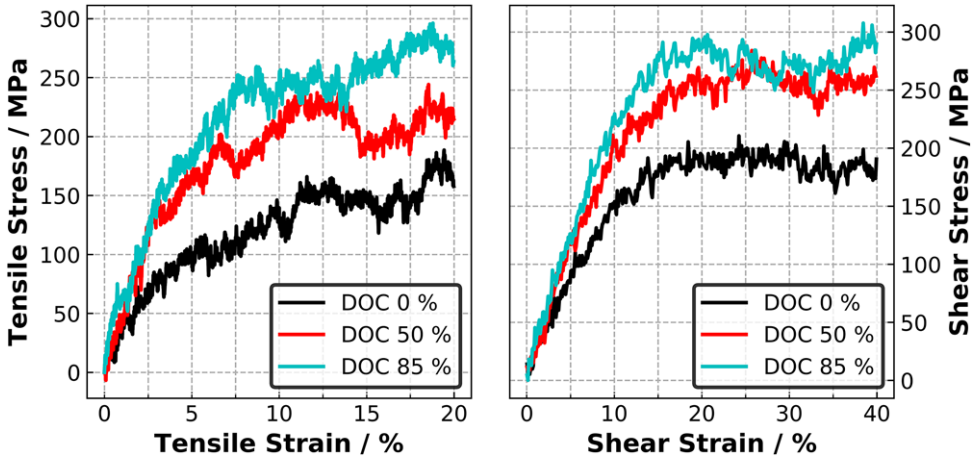

Figure 4. Predicted mechanical response of cross-linked hydrogel samples with a sample size of 1 uc (details in Section 2) and a water loading of 10 wt%, at different degrees of cross-linking. a) Tensile stress versus strain data. b) Shear stress versus strain data.

the polymer content (i.e., the content of the PAAm oligomers and MBAm molecules in this case) of the hydrogel samples investigated here is a key parameter in the formation of elastic hydrogels because the gelation occurs through cross-linking of the polymer chains with the cross-linkers. We remark here that merely increasing the non-water content (i.e., the PAAm and MBAm in our case) in the hydrogel sample does not necessarily guarantee a sample with better elastic properties. We propose that the formation of cross-link bonds between the PAAm oligomers and the MBAm cross-linkers is a key contributor here to impart elasticity.

However, the polymer content is not the only parameter that can contribute to the elastic behavior of the hydrogels. Hydrogels with very high water uptake (even up to around 99 wt%) are reported to be mechanically robust.[74–76] For instance, Li et al. experimentally measured the tensile strength and elongation at the yield point of a photo-cured polyurethane hydrogel and demonstrated that the increase in viscosity due to the conformational change of the photo-responsive molecules (e.g., cis–trans isomerization) contributed to the stiffness of the hydrogel.[76]

Since we have already predicted that the hydrogel samples with water contents of 50 and 90 wt% feature limited elasticity (Figure 3), we focused on hydrogel samples with 10 wt% water content to elucidate the effect of the DOC. **Figure 4**a provides the tensile SSCs for the hydrogel samples at 10 wt% water content and at different DOC values. Our data suggest that at 10 wt% water loading, the uncured hydrogel sample (i.e., DOC of 0%, comprising a liquid mixture of un-cross-linked pre-polymerized PAAm and MBAm molecules) had an appreciable elastic behavior under tensile deformation. The Young's modulus of this uncured hydrogel was 2.84 GPa. We attribute this to the presence of the pre-polymerized PAAm oligomers in the uncured hydrogel samples. However, we expect that the formation of a 3D bonding network can impart mechanical enhancement relative to the uncured hydrogel. With an increase in DOC to 50%, the tensile response of the hydrogel increased by almost 60%, to 4.59 GPa. A further enhancement was obtained for a DOC of 85%, where the Young's modulus was predicted to be 4.84 GPa, a 70% increase in Young's modulus compared to the uncured hydrogel sample.

For reference, the experimental values for Young's modulus of the PAAm–MBAm hydrogel are reported to vary between ≈110–200 MPa for different PAAm-to-MBAm ratios.[77] However, we note that the DOC of these experimentally studied PAAm–MBAm hydrogels is not necessarily known or explicitly reported. In addition, we expect that the difference between experimentally accessible strain rates and computationally practical strain rates will give rise to discrepancies between the measured and predicted absolute values of mechanical properties such as Young's modulus. An experimental study conducted by Xia et al.[75] showed a trend that is consistent with our predictions, in that the Young's modulus of a nanostructured smart hydrogel based on poly(NiPAM), MBAm, and *N,N,N′,N′*-tetramethylethylenediamine increased with the concentration of the NiPAM monomers in the sample. These authors attributed this enhancement in Young's modulus to an increase in the extent of the 3D polymeric network in the sample.

We also investigated our hydrogel samples under shear deformation. Based on the outcomes of our tensile tests, we only considered hydrogel samples with a water content of 10 wt% at different DOC values. Figure 4b shows the predicted shear stress values as a function of the shear strain for the three DOC values, indicating that the uncured hydrogel sample (i.e., DOC 0%) exhibited an appreciable shear response. Similar to the high tensile response of the uncured hydrogel sample, this high shear response of the uncured hydrogel sample could be explained by the presence of the pre-polymerized PAAm oligomers in the hydrogel sample. Increasing the DOC conferred a positive effect on the shear response of the hydrogel, such that the DOC 85% sample exhibited the greatest shear response of the three. The predicted shear modulus of the DOC 85% sample was 2.94 GPa, while that of the uncured hydrogel sample (i.e., DOC 0%) was 1.99 GPa. A DOC of 50% yielded an intermediate shear modulus value of 2.43 GPa. **Figure 5** summarizes our predicted Young's modulus and shear modulus values.

Our shear deformation findings are consistent with experimentally reported results in the literature.[78–80] In a related study, Jiang et al.[78] reported the experimentally determined shear

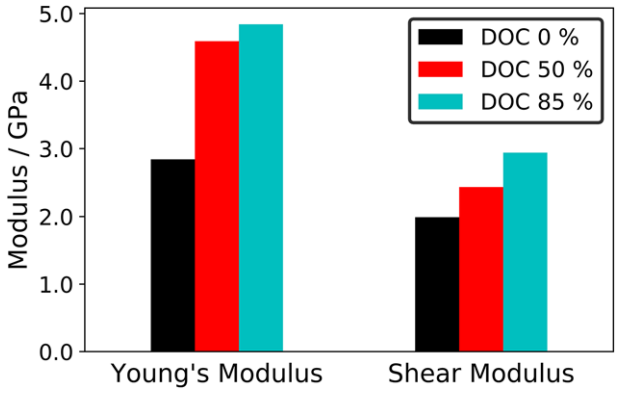

Figure 5. Predicted Young's and shear modulus values for the hydrogel samples with sample size of 1 uc (details in Section 2) and a water content of 10 wt% at different degrees of cross-linking.

response of an AAm-based hydrogel as a function of the cross-linking density. However, we note that these authors indirectly inferred the cross-linking density via back-calculation of the effective network chain density using the shear modulus values. These authors reported that the increase in the shear viscosity as a response to the increased cross-linking density led to an increase in the shear modulus of the hydrogel. As already indicated earlier, the shear rate can influence the absolute shear response of the hydrogel. Nesrinne and Djamel[80] reported the experimentally measured shear rate dependence of acrylic acid (AA)-AAm hydrogels. These authors found that the shear stress of these hydrogels increased (but not linearly) with an increase in the shear rate due to an increase in the viscosity (i.e., typical behavior of shear-thickening fluids). In our MD simulations, we implemented a shear strain rate and a tensile strain rate that were several orders of magnitude faster than the experimentally accessible deformation rates. For example, the tensile strain rate used here was 5×10^{7} s^{-1}, whereas the experimental tensile strain rate implemented in ref. [79] was 2×10^{-2} s^{-1}. This limitation is chiefly due to the computational resources required to capture slower strain rates (i.e., it is theoretically possible to test the hydrogel samples with the experimental shear rates/tensile rates using MD simulations, but this would not be practical in terms of the required time to complete these simulations). Here, we did not investigate the influence of deformation rate on the mechanical response of our hydrogels. Although the strain rate implemented in both experiments and MD simulations can influence the absolute value of the moduli, we are chiefly interested in the *trend* in modulus values calculated using MD simulations, not the absolute values.

Moreover, we used a traditional all-atom FF in our simulations, namely OPLS.[81] This FF assumes a fixed bonding topology and does not allow for us to model bond breakage as a response to applied strain. For example, the experimental elongation at breakage for our hydrogel sample was at ≈11% of strain[47] and from 1–4.5% of strain,[77] whereas our simulations went up to 20% of strain without showing any failure, likely due to this limitation of the FF. Such limitations can be obviated by, for example, the use of 0.2% offset line.[40] Our predicted yield strain values mirrored the trend that was observed in our Young's modulus values. With the use of this 0.2% offset line, the yield strain values were predicted to be around 2.8, 3.1, and 3.4% for the hydrogel samples with the water content of 10 wt% and with DOC values of 0%, 50%, and 85%, respectively. This offset line analysis enabled us to predict the relationship between DOC and yield point of the hydrogel. Therefore, rather than the absolute values of the yield strain and yield stress, the *trend* in these values is of chief interest here.

We recognize that varying the ratio of the number of constituent molecules (in our case pre-polymerized PAAm and MBAm) can produce differing hydrogel properties.[80,82] For instance, Yang et al.[82] varied the ratio of AA and AAm of a co-monomer hydrogel and experimentally measured its tensile response. Their results suggested that an increase in the AA/AAm ratio in favor of AAm increased the modulus, while the elongation at failure was reduced.[82] Here, we have investigated a fixed value of the PAAm/MBAm ratio of 0.25. Investigation of the effect of the PAAm/MBAm ratio on the thermo-mechanical properties would be a fruitful direction for future study.

3.2. Thermal Conductivity of Hydrogels

In addition to the mechanical properties of our hydrogels, we explored how the length of pre-polymerized PAAm oligomer, the DOC, and the water content affected the thermal transport properties of the hydrogel samples with a system size of 1 uc. Furthermore, we also elucidated the effect of the system size (i.e., 4 and 8 uc) on the thermal conductivity at different DOC values.

We first explored the effect of the length of pre-polymerized PAAm oligomer on the thermal conductivity. We tested three pre-polymerized PAAm oligomer lengths comprising 10-, 16-, and 32-units of AAm at DOC values of 0% and 85%, using the 1-uc system size. Our results, provided in Figure S2, Supporting Information, indicate that the thermal conductivity of the hydrogel samples did vary appreciably as a function of PAAm oligomer length, within the range investigated here. Based on these findings, we focused our thermal conductivity calculations on the samples generated from the 10-mer long PAAm oligomers. We remark here that the use of larger MD simulation cells may affect the dependence of PAAm oligomer size on the thermal conductivity. However, we are chiefly interested in the *trend* in thermal conductivities as a function of DOC and water content. Work in our labs is currently underway to develop a computational procedure that will facilitate the polymerization of the AAm monomers in situ. Such developments will enable a deeper investigation of the influence of the PAAm oligomer length on hydrogel thermal properties. We also investigated the dependence of the thermal conductivity on the principal direction along which it was calculated. These tests were performed for a larger system size, 4 uc, as detailed in Section 2. Justification for this choice of the system size for these test calculations is addressed below. In Figure S3, Supporting Information, we provide the thermal conductivity values for the 4-uc hydrogel sample with a water content of 50 wt% and a DOC of 85%, which indicate that the thermal conductivity was invariant to the direction of calculation (as expected).

In **Figure 6**a, we provide calculated thermal conductivity values as a function of water loading for DOC values of 0% and 85% and a system size of 1 uc. These data suggest that the

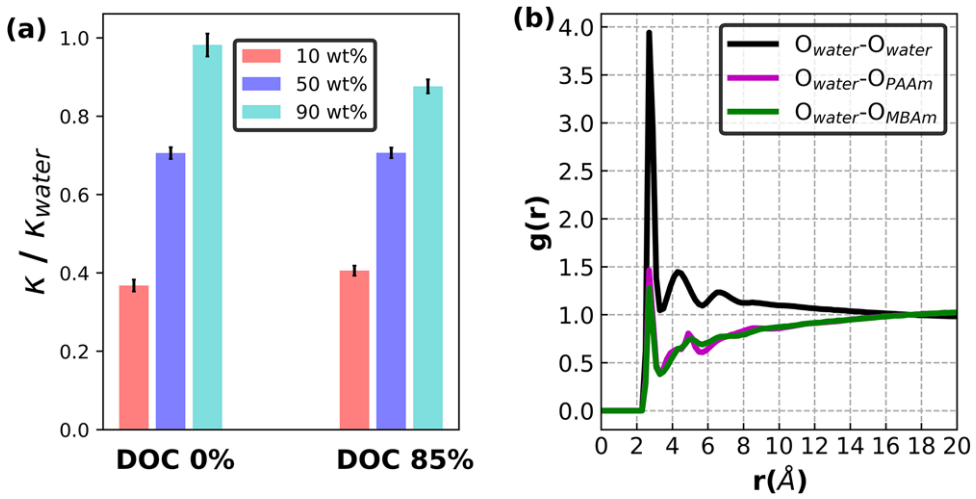

Figure 6. a) Thermal conductivities of uncured (DOC 0%) and cross-linked hydrogel samples using a system size of 1 uc at 300 K with different water loadings. b) RDF plots, g(r), for the hydrogel oxygen atoms; sample size of 1 uc with a DOC of 50% and water loading of 50 wt%.

thermal conductivity of the hydrogels increased with increasing water content, regardless of whether the sample was uncured or cross-linked (we reiterate here that we define a DOC of 0% to correspond to a system of un-crosslinked MBAm molecules and pre-polymerized PAAm oligomers). For instance, the predicted thermal conductivity increased almost monotonically, from 0.30 to 0.98 W m^{-1} K^{-1} with water content from 0% to 100% for a DOC of 0%. Typical normalized heat current autocorrelation functions for these hydrogel samples are provided in Figure S4, Supporting Information.

Our predicted thermal conductivity for pure liquid water (0.98 ± 0.04 W m^{-1} K^{-1}) is consistent with previous modeling studies.[83,84] This value is higher than that of experimental measurement[21] of 0.60 W m^{-1} K^{-1}, which is associated with the empirical force fields used in the MD simulations. Romer[83] showed that TIP4P and SPC/E water models yielded similar thermal conductivities for pure water at a given temperature. These authors also suggested that the water models used in MD simulations typically gave rise to thermal conductivities greater than the experimental values at a given thermodynamic state. This was ascribed to the fact that many (but not all) widely used water models were not explicitly parameterized using thermal conductivity data, but with reference to other properties such as liquid density[85] and enthalpy of vaporization.[86]

We attribute the beneficial effect of water loading on the thermal conductivity to the extent of hydrogen-bonding network in the hydrogel samples. To elucidate this, we report RDFs (Figure 6b) for the O_{H2O}-O_{H2O}, O_{H2O}-O_{PAAm}, and O_{H2O}-O_{MBAm} pairs. These RDFs in Figure 6b were calculated for a hydrogel sample size of 1 uc with a water content of 50 wt% and a DOC of 50%. We chose a DOC of 50% (which is intermediate between the uncured and highly cured hydrogel samples) for the purpose of observing the trend. As is clearly seen in Figure 6b, the amplitude of the first peak for O_{H2O}-O_{H2O} was the greatest among the three pairs, which, in turn, reflected the dominant effect of the interactions between water molecules on the thermal conductivity. All three RDFs summarized in Figure 6b yielded a peak position at around 2.7 Å, which implies the formation of hydrogen-bonding network between the pairs (e.g., the PAAm and water molecules).[87–90] The highest thermal conductivity was predicted for the pure liquid water sample, which also underscores the importance of the presence of hydrogen bonds.

We also calculated the water coordination number (CN) for the hydrogel using a system size of 1 uc, a water loading of 50 wt%, and a DOC of 50%. For comparison, we also calculated the water CN in our pure water sample. The CN was defined to be the average number of water molecules found in the first solvation shell, calculated by integrating the relevant RDF out to the first trough (i.e., from r = 0 to ≈3.5 Å, Figure 6b). Our results revealed that the water CNs predicted for the hydrogel sample and pure water sample were 4.5 and 4.7, respectively. These results suggest that in the hydrogel sample, slightly fewer water molecules were coordinated with each other, which in turn yielded a lower thermal conductivity compared to that predicted for pure water. Our water CN for the pure water sample was also in good agreement with the experimental (4.50)[91] and predicted (4.59)[92] results. Unfortunately, there are no experimental CN data for the PAAm–MBAm hydrogel system available in the literature. In a related study, Lee et al.[36] predicted the water CN for various atomic site pairs in poly(*N*-vinyl-2-pyrrolidone-*co*-2-hydroxyethyl methacrylate) hydrogels using MD simulations. These authors reported an increase in water CN at higher water loadings. This fact can account for the higher thermal conductivities in the hydrogel samples with high water content because the heat is mainly conducted from the polymer to the water molecules by the vibrations of the water molecules surrounding the polymer chains.

We ascribe our predicted increase in thermal conductivity with increasing water content to the ability of water molecules to conduct heat through hydrogen bond networks.[93] As detailed in Section 2, we estimated the size of the water clusters, which may serve as a useful metric in this respect. Water molecules in close spatial contact are expected to conduct heat more efficiently, and an increase in the number of water molecules in such contact would conceivably augment heat transfer. Therefore, we first determined the optimal number of water clusters in our hydrogel samples. We performed this initial analysis by setting

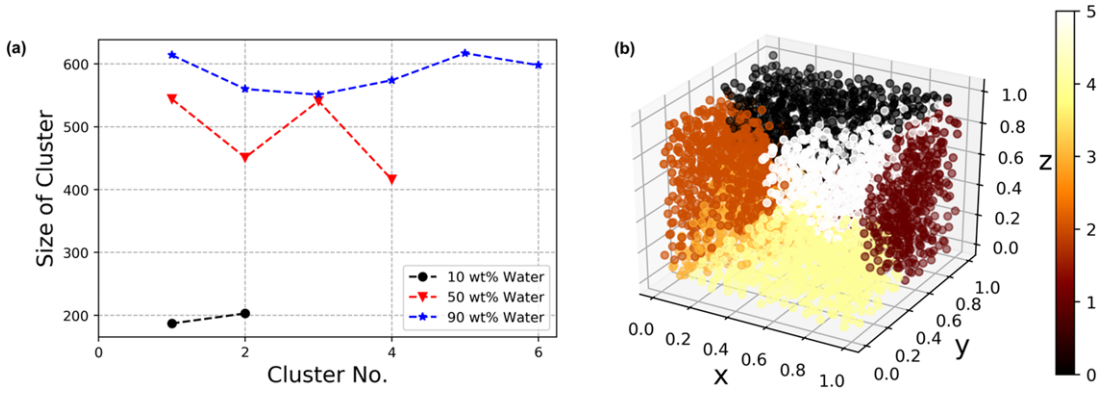

Figure 7. a) Predicted optimal number of clusters and cluster size for each hydrogel sample. b) Scatter plot for the spatial distribution of clusters of water in the hydrogel sample size of 1 uc, a DOC of 50%, and a water loading of 50 wt%. *x*, *y*, and *z* represent the normalized dimensions of the simulation cell. The color map indicates the cluster number related to part (a).

the number of clusters to 20. We report our predicted cluster size for each cluster found in each type of hydrogel sample, as shown in Figure S5a, Supporting Information. Our results suggest that the hydrogel sample with the highest water loading investigated here featured larger water clusters. This result is not unexpected, given that a greater number of water molecules are present in the hydrogel with higher water loading. Therefore, we expect that a greater number of larger water clusters should contribute to an enhanced thermal conductivity of the hydrogel. On the other hand, for the samples with low water loading, the formation of small water clusters is expected; these water clusters might show different behavior if they are confined within the cross-linked polymer network. This confinement might lead to locally varying physical properties for these water clusters (e.g., interfacial tension) within the sample. Future studies warrant a close examination of this via experimental techniques and computational approaches.[94]

We next sought to estimate the optimal number of clusters, by predicting how the total SSE varied with the number of predicted clusters and using the elbow method (Figure S5b, Supporting Information). We found that the resulting optimal number of clusters was dependent on the water loading of the hydrogel sample. For a DOC of 50%, two clusters were predicted to be optimal for the hydrogel sample with 10 wt% loading, whereas four and six clusters were optimal for 50 wt% and 90% wt water content, respectively (**Figure 7**a). Figure 7b shows the scatter plot for the water clusters calculated for a hydrogel sample of size 1 uc, with water content of 90 wt% and a DOC of 50%. Different colors indicate the water oxygen atoms belonging to different clusters (six clusters in total).

For a DOC of 50%, when the water content was relatively low (such as 10 wt%), the available water molecules mostly formed small clusters. On the other hand, a relatively high water content (e.g., 90 wt%) yielded a predicted network between water molecules that was similar with that predicted for the pure water sample. In the case of the 50% DOC hydrogel with 50 wt% water content, our data indicate the presence of more regions where water molecules can reside and potentially become trapped, which in turn would logically lead to a relatively higher optimal number of water clusters in the hydrogel. We reiterate here that we analyzed only one snapshot, which was the equilibrated frame that was also used as the basis for our computational mechanical testing, for each hydrogel sample.

As already indicated earlier, we propose that under certain conditions, the predicted thermal conductivity of the hydrogel sample may be influenced by the MD simulation cell size, particularly in a size range inclusive of small system sizes. We base this suggestion on a consideration of the relative length-scales of the cell dimensions versus the length-scale of the average segment chain-length between cross-link points along the PAAm chain in the cured hydrogel. To elaborate, we suspect that such system-size effects may be at their most acute for the case where the crosslink-to-crosslink length-scale is comparable to the simulation cell dimensions. In this scenario, we suggest that the polymer network might not be appropriately represented, which might then have a detrimental impact on the predicted thermal conductivity. Consider that our thermal conductivity calculations were performed using hydrogel samples containing a fixed length of PAAm oligomer (10-mer) which has an idealized (fully extended) chain length of approximately 30 Å. Given that the 1-uc simulation cell dimensions were approximately 46–49 Å, the average crosslink-to-crosslink length-scale had the potential to be almost comparable to the simulation cell dimensions, which therefore suggests that system-size effects could potentially be significant. To gauge this, in **Figure 8**a, we report our predicted thermal conductivities as a function of system size and DOC, for a water content of 50 wt%. As expected, our predicted thermal conductivities for the un-crosslinked sample (we reiterate that a DOC = 0%, i.e., "un-crosslinked" refers to a sample containing a mixture of pre-polymerized PAAm 10-mers and MBAm monomers that are not connected by covalent bonds) showed no appreciable dependence on the size of simulation cell. However, the results for the samples with DOC of 85% indicated a clear system-size dependency in the predicted thermal conductivity comparing 1 uc to 4 uc, but no appreciable dependence when comparing 4 uc with 8 uc. Overall, for a fixed PAAm oligomer length of ten repeat units, our data indicate that the ideal smallest system size for the calculation of thermal conductivity should be at least 4 uc. Based on the 4-uc system size, the thermal conductivities increased with DOC, from 0.69 ± 0.03 W m^{-1} K^{-1} for a DOC of 0% to 0.83 ± 0.04 W m^{-1} K^{-1} for a DOC of 85%.

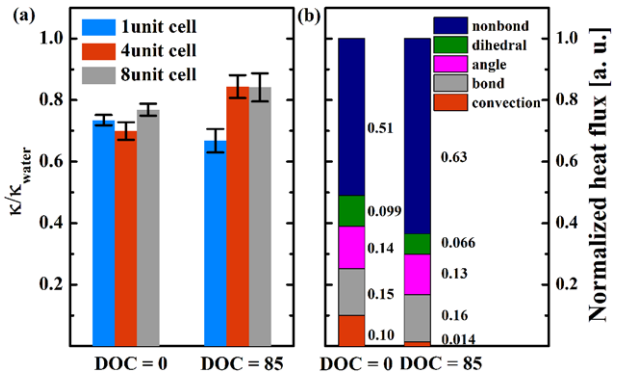

Figure 8. a) System-size (1 uc, 4 uc, 8 uc; see text for details) dependence of the predicted thermal conductivity calculated via equilibrium molecular dynamics simulations with different degrees of cross-linking. The water content of these samples was 50 wt%. b) Normalized heat flux contributions from non-bonding (van der Waals and Coulombic interactions), bond, angle, dihedral, and convection terms at different DOCs, calculated using non-equilibrium molecular dynamics for a sample size of 4 uc and a water loading of 50 wt%.

As detailed earlier, we investigated the dependence of predicted thermal conductivity on PAAm oligomer chain length (namely 10-, 16-, or 32-mers) by using our smallest sample size (i.e., 1 uc); we observed no apparent influence on thermal conductivity in this instance. However, based on our arguments and findings drawn from Figure 8a, namely that the minimum sample size to calculate the thermal conductivity should be at least 4 uc, we propose that the effect of PAAm oligomer chain length might influence the thermal conductivity if larger simulation cells were used. This will be investigated in future work.

To further reveal how the DOC influenced hydrogel thermal conductivity, we partitioned the total heat flux that was used to determine the thermal conductivity into its components based on the type of interatomic interaction. This partitioning provided contributions based on the non-bonded interaction terms (i.e., the sum of the van der Waals and Coulombic interactions) and bonded interaction terms (such as the bond stretching, angle bending, dihedral, and convection terms). To achieve this, we used NEMD and investigated two samples: uncured (DOC of 0%) and cured (DOC of 85%) with a water content of 50 wt% and a system size of 4 uc, for the system comprising pre-polymerized PAAm 10-mers. A typical NEMD simulation cell is illustrated in Figure S6, Supporting Information. As shown in Figure 8b, the non-bonded heat flux comprises the dominant contribution for both DOC values. Furthermore, this non-bonded contribution was greater for the cured sample compared to the uncured sample. We attribute this to the formation of covalent cross-link bonds between the PAAm oligomers and MBAm molecules, which we propose resulted in closer intermolecular non-covalent contact. This can concomitantly lead to more favorable intermolecular interactions and thus enhanced thermal transport. Our findings here, regarding the beneficial effects of the formation of new covalent bonds on thermal conductivity in hydrogels, are consistent with published simulation data on amorphous polymers.[71,95]

Our results also revealed that the formation of cross-link bonds did not significantly alter the normalized proportion of the bonded heat flux contribution to the total heat flux when comparing the uncured and cured samples. Again, because our sample comprised pre-polymerized PAAm 10-mers, the difference in the number of new covalent bonds when comparing 0% DOC with 85% DOC is actually quite small. To illustrate this, consider an example system with a water content of 50 wt% and a system size of 1 uc. At a DOC of 50%, the number of new cross-link bonds formed between the PAAm 10-mers and MBAm molecules will be 32 (in this case, the system contained 32 PAAm 10-mers and each has two reactive sites situated at both ends); 32 new covalent bonds correspond to ≈0.3% of the total bonds present in the simulation cell. In future work, we will adapt our cross-linking procedure to facilitate in situ oligomerization of the PAAm during the MD simulations. This would provide a clearer benchmark between truly uncured and fully cured samples.

Moreover, the proportion of the convection contribution term was almost an order of magnitude smaller in the cross-linked sample compared with the uncured system. We propose this reduction can be attributed to the restricted mobility of the molecules in the cured sample. With the increase in DOC, the hydrogel samples became more solid-like; this solidification can broadly limit the mass transport of molecules in the sample,[96] particularly in terms of mobility of the water content. Specifically, we suggest that the cross-linked polymer constituent of the hydrogel (the cross-linked PAAm–MBAm in our case) can form pockets or voids, which can trap aggregates of water molecules and frustrate their subsequent translational diffusion through the sample.[97,98] Since the water molecules can undergo translational motion less freely in the cured hydrogel compared to the uncured sample,[27] the proportional contribution of the convection term to the heat flux in the cured sample will be less. Our computational findings are consistent with published experimental observations, as reported for poly(NiPAM) hydrogels[99] and poly (methacrylic acid) hydrogels.[100]

4. Summary and Conclusions

We predicted thermo-mechanical properties of PAAm–MBAm hydrogels as a function of various structural and compositional parameters, based on all-atom molecular dynamics simulations. Our predictions were broadly consistent with reported experimental data. Our findings reveal the molecular-level complexity between hydrogel water content and DOC , both of which are associated with the thermo-mechanical performance of these materials. We predicted that the fraction of polymer content is a key determinant in conferring elasticity to the hydrogel. Our results also suggested that water content has a strong role in conferring higher thermal conductivities to the hydrogel. Our simulation results indicated a proportionally greater contribution due to non-bonding interactions (i.e., the vdW and Coulombic interactions) to the heat flux relative to bonding interactions, for cured samples compared with uncured samples. Moreover, the convection contribution to the thermal transport, related to the ability of water molecules to translationally diffuse through the hydrogel, was found to be substantially reduced for higher degrees of cross-linking. Our analysis also suggested that the spatial range and distribution of water aggregates in the hydrogel can exert a strong

influence on heat conduction through the hydrogen-bonding network in the hydrogel.

We used pre-polymerized PAAm oligomers as the basis of our computational sample preparation. This was due to limitations in current computational procedures needed to capture radical polymerization using traditional molecular dynamics simulations and all-atom force fields. Current work in our labs to develop such a radical polymerization computational procedure is underway and will provide a basis for future hydrogel studies. Such advances will enable a more detailed elucidation of the contributions to the thermo-mechanical properties of these hydrogels. Our computational procedure and findings provide a rational, knowledge-based foundation for ultimately proposing, designing, and testing novel, customized hydrogels for specific and bespoke applications.

Supporting Information

Supporting Information is available from the Wiley Online Library or from the author.

Acknowledgements

M.A. and B.D. contributed equally to this work. The work was supported by the National Natural Science Foundation of China (Grant Nos. 51576076, 51711540031), the Natural Science Foundation of Hubei Province (No. 2017CFA046), the Fundamental Research Funds for the Central Universities (2016YXZD006), and Natural Science Research Start-up Fund of Shaanxi University of Science and Technology (2018GBJ-10). This work was also partially supported by the Australian Research Council via grant DP180100094. The authors thank the National Supercomputing Center in Tianjin (NSCC-TJ) and China Scientific Computing Grid (ScGrid) for providing assistance in computations. T.R.W. gratefully acknowledges computational resources provided by the National Computational Infrastructure (NCI) and the Pawsey Supercomputing Centre.

Conflict of Interest

The authors declare no conflict of interest.

Keywords

cross-linking, hydrogels, molecular dynamics simulations, polyacrylamides, thermal conductivity

Received: October 6, 2018
Revised: November 29, 2018
Published online: January 4, 2019

[1] X. Zhao, *Soft Matter* **2014**, *10*, 672.
[2] F. Ullah, M. B. H. Othman, F. Javed, Z. Ahmad, H. M. Akil, *Mater. Sci. Eng. C* **2015**, *57*, 414.
[3] M. P. Lutolf, J. A. Hubbell, *Nat. Biotechnol.* **2005**, *23*, 47.
[4] Y. Jiang, J. Chen, C. Deng, E. J. Suuronen, Z. Zhong, *Biomaterials* **2014**, *35*, 4969.
[5] N. A. Peppas, J. Z. Hilt, A. Khademhosseini, R. Langer, *Adv. Mater.* **2006**, *18*, 1345.
[6] M. M. Pakulska, K. Vulic, R. Y. Tam, M. S. Shoichet, *Adv. Mater.* **2015**, *27*, 5002.
[7] Y. Cheng, L.-D. Koh, F. Wang, D. Li, B. Ji, J. Yeo, G. Guan, M.-Y. Han, Y.-W. Zhang, *Nanoscale* **2017**, *9*, 9181.
[8] G. Maurdev, R. Millington Keith, *J. Appl. Polym. Sci.* **2009**, *113*, 2346.
[9] S. Lin, H. Yuk, T. Zhang, G. A. Parada, H. Koo, C. Yu, X. Zhao, *Adv. Mater.* **2016**, *28*, 4497.
[10] Y. Shi, L. Pan, B. Liu, Y. Wang, Y. Cui, Z. Bao, G. Yu, *J. Mater. Chem. A* **2014**, *2*, 6086.
[11] G. Chen, N. Matsuhisa, Z. Liu, D. Qi, P. Cai, Y. Jiang, C. Wan, Y. Cui, W. R. Leow, Z. Liu, S. Gong, K.-Q. Zhang, Y. Cheng, X. Chen, *Adv. Mater.* **2018**, *30*, 1800129.
[12] H. Yuk, S. Lin, C. Ma, M. Takaffoli, N. X. Fang, X. Zhao, *Nat. Commun.* **2017**, *8*, 14230.
[13] F. Zhu, L. Cheng, Z. J. Wang, W. Hong, Z. L. Wu, J. Yin, J. Qian, Q. Zheng, *ACS Appl. Mater. Interfaces* **2017**, *9*, 11363.
[14] F. Zhao, X. Zhou, Y. Shi, X. Qian, M. Alexander, X. Zhao, S. Mendez, R. Yang, L. Qu, G. Yu, *Nat. Nanotechnol.* **2018**, *13*, 489.
[15] J. Y. Sun, X. Zhao, W. R. Illeperuma, O. Chaudhuri, K. H. Oh, D. J. Mooney, J. J. Vlassak, Z. Suo, *Nature* **2012**, *489*, 133.
[16] X. Zhao, *Proc. Natl. Acad. Sci.* **2017**, *114*, 8138.
[17] X. Zhao, *Soft Matter* **2014**, *10*, 672.
[18] J. P. Gong, Y. Katsuyama, T. Kurokawa, Y. Osada, *Adv. Mater.* **2003**, *15*, 1155.
[19] J. P. Gong, *Soft Matter* **2010**, *6*, 2583.
[20] H. Yuk, T. Zhang, S. Lin, G. A. Parada, X. Zhao, *Nat. Mater.* **2016**, *15*, 190.
[21] N. Tang, Z. Peng, R. Guo, M. An, X. Chen, X. Li, N. Yang, J. Zang, *Polymers* **2017**, *9*, 688.
[22] F. Xiao, S. Naficy, G. Casillas, M. H. Khan, T. Katkus, L. Jiang, H. Liu, H. Li, Z. Huang, *Adv. Mater.* **2015**, *27*, 7196.
[23] M. D. Bartlett, N. Kazem, M. J. Powell-Palm, X. Huang, W. Sun, J. A. Malen, C. Majidi, *Proc. Natl. Acad. Sci. USA* **2017**, 201616377.
[24] C. Li, Y. Ma, Z. Tian, *ACS Macro Lett.* **2018**, *7*, 53.
[25] D. G. Cahill, R. O. Pohl, *Phys. Rev. B* **1987**, *35*, 4067.
[26] C. Wu, *Polymer* **2010**, *51*, 4452.
[27] Y. Wu, S. Joseph, N. Aluru, *J. Phys. Chem. B* **2009**, *113*, 3512.
[28] Y. Tamai, H. Tanaka, K. Nakanishi, *Macromolecules* **1996**, *29*, 6750.
[29] P. A. Netz, T. Dorfmüller, *J. Phys. Chem. B* **1998**, *102*, 4875.
[30] C. Oldiges, T. Tonsing, *Phys. Chem. Chem. Phys.* **2000**, *2*, 5630.
[31] T. Tonsing, C. Oldiges, *Phys. Chem. Chem. Phys.* **2001**, *3*, 5542.
[32] G. Longhi, F. Lebon, S. Abbate, S. L. Fornili, *Chem. Phys. Lett.* **2004**, *386*, 123.
[33] S. Deshmukh, D. A. Mooney, J. M. D. Macelroy, *Mol. Simul.* **2011**, *37*, 846.
[34] S. Mani, F. Khabaz, R. V. Godbole, R. C. Hedden, R. Khare, *J. Phys. Chem. B* **2015**, *119*, 15381.
[35] S. S. Jang, W. A. Goddard, M. Y. S. Kalani, *J. Phys. Chem. B* **2007**, *111*, 1729.
[36] S. G. Lee, G. F. Brunello, S. S. Jang, D. G. Bucknall, *Biomaterials* **2009**, *30*, 6130.
[37] S. G. Lee, G. F. Brunello, S. S. Jang, J. H. Lee, D. G. Bucknall, *J. Phys. Chem. B* **2009**, *113*, 6604.
[38] S. Mathesan, A. Rath, P. Ghosh, *Mater. Sci. Eng.: C* **2016**, *59*, 157.
[39] S. Xu, S. Cai, Z. Liu, *ACS Appl. Mater. Interfaces* **2018**, *10*, 36352.
[40] B. Demir, T. R. Walsh, *Soft Matter* **2016**, *12*, 2453.
[41] B. Demir, L. C. Henderson, T. R. Walsh, *ACS Appl. Mater. Inter.* **2017**, *9*, 11846.
[42] B. Demir, K. M. Beggs, B. L. Fox, L. Servinis, L. C. Henderson, T. R. Walsh, *Compos. Sci. Technol.* **2018**, *159*, 127.
[43] M. Laurien, B. Demir, H. Büttemeyer, A. Herrmann, T. Walsh, L. Ciacchi, *Macromolecules* **2018**, *51*, 3983.
[44] B. Tamanna, N. A. K., S. Reena, *J. Appl. Polym. Sci.* **2003**, *89*, 779.
[45] J.-Y. Sun, X. Zhao, W. R. Illeperuma, O. Chaudhuri, K. H. Oh, D. J. Mooney, J. J. Vlassak, Z. Suo, *Nature* **2012**, *489*, 133.

[46] H. Yuk, T. Zhang, G. A. Parada, X. Liu, X. Zhao, *Nat. Commun.* **2016**, *7*, 12028.
[47] N. Rauner, M. Meuris, M. Zoric, J. C. Tiller, *Nature* **2017**, *543*, 407.
[48] W. L. Jorgensen, D. S. Maxwell, J. Tirado-Rives, *J. Am. Chem. Soc.* **1996**, *118*, 11225.
[49] W. L. Jorgensen, J. D. Madura, *Mol. Phys.* **1985**, *56*, 1381.
[50] M. W. Mahoney, W. L. Jorgensen, *J. Chem. Phys.* **2000**, *112*, 8910.
[51] J.-P. Ryckaert, G. Ciccotti, H. J. Berendsen, *J. Comput. Phys.* **1977**, *23*, 327.
[52] S. Nosé, *J. Chem. Phys.* **1984**, *81*, 511.
[53] W. G. Hoover, *Phys. Rev. A* **1985**, *31*, 1695.
[54] W. G. Hoover, *Phys. Rev. A* **1986**, *34*, 2499.
[55] R. W. Hockney, J. W. Eastwood, *Computer Simulation Using Particles*, CRC Press, Boca Raton, FL **1988**.
[56] S. Plimpton, *J. Comput. Phys.* **1995**, *117*, 1.
[57] X. Shaofeng, S. Frantisek, F. J. M. J., *J. Polym. Sci. A1* **1997**, *35*, 1013.
[58] S. Xie, F. Svec, J. M. J. Fréchet, *J. Chem. Theory Comput.* **2007**, *3*, 2312.
[59] Y. Li, Z. Dong, *J. Chem. Inf. Model.* **2016**, *56*, 1205.
[60] T. D. Huan, R. Batra, J. Chapman, S. Krishnan, L. Chen, R. Ramprasad, *npj Comput. Mater.* **2017**, *3*, 37.
[61] L. Li, Y. Yang, D. Zhang, Z.-G. Ye, S. Jesse, S. V. Kalinin, R. K. Vasudevan, *Sci. Adv.* **2018**, *4*,.
[62] Y. Matsunaga, Y. Sugita, *J. Chem. Phys.* **2018**, *148*, 241731.
[63] F. Pedregosa, G. Varoquaux, A. Gramfort, V. Michel, B. Thirion, O. Grisel, M. Blondel, P. Prettenhofer, R. Weiss, V. Dubourg, J. Vanderplas, A. Passos, D. Cournapeau, M. Brucher, M. Perrot, E. Duchesnay, *J. Mach. Learn. Res.* **2011**, *12*, 2825.
[64] http://scikit-learn.org/Stable/Modules/Generated/Sklearn.Cluster.Kmeans.Html, accessed: 1 June 2018.
[65] P. K. Schelling, S. R. Phillpot, P. Keblinski, *Phys. Rev. B* **2002**, *65*, 144306.
[66] X.-Y. Mi, X. Yu, K.-L. Yao, X. Huang, N. Yang, J.-T. Lü, *Nano Lett.* **2015**, *15*, 5229.
[67] D. Ma, H. Ding, H. Meng, L. Feng, Y. Wu, J. Shiomi, N. Yang, *Phys. Rev. B* **2016**, *94*, 165434.
[68] M. An, Q. Song, X. Yu, H. Meng, D. Ma, R. Li, Z. Jin, B. Huang, N. Yang, *Nano Lett.* **2017**, *17*, 5805.
[69] Q. Song, M. An, X. Chen, Z. Peng, J. Zang, N. Yang, *Nanoscale* **2016**, *8*, 14943.
[70] J. H. Irving, J. G. Kirkwood, *J. Chem. Phys.* **1950**, *18*, 817.
[71] D. Torii, T. Nakano, T. Ohara, *J. Chem. Phys.* **2008**, *128*, 044504.
[72] X. Wei, T. Zhang, T. Luo, *Phys. Chem. Chem. Phys.* **2016**, *18*, 32146.
[73] T. Zhang, T. Luo, *J. Phys. Chem. B* **2016**, *120*, 803.
[74] E. A. Appel, X. J. Loh, S. T. Jones, F. Biedermann, C. A. Dreiss, O. A. Scherman, *J. Am. Chem. Soc.* **2012**, *134*, 11767.
[75] L.-W. Xia, R. Xie, X.-J. Ju, W. Wang, Q. Chen, L.-Y. Chu, *Nat. Commun.* **2013**, *4*, 2226.
[76] J. Li, L. Ma, G. Chen, Z. Zhou, Q. Li, *J. Mater. Chem. B* **2015**, *3*, 8401.
[77] J.-Y. Sun, X. Zhao, W. R. K. Illeperuma, O. Chaudhuri, K. H. Oh, D. J. Mooney, J. J. Vlassak, Z. Suo, *Nature* **2012**, *489*, 133.
[78] J. Guoqing, H. Li, L. Bo, L. Changsen, L. Rui, L. Fengqi, *J. Appl. Polym. Sci.* **2012**, *123*, 66.
[79] A. D. Drozdov, J. D. Christiansen, *Int. J. Solids Struct.* **2013**, *50*, 3570.
[80] S. Nesrinne, A. Djamel, *Arabian J. Chem.* **2017**, *10*, 539.
[81] W. L. Jorgensen, D. S. Maxwell, J. Tirado-Rives, *J. Am. Chem. Soc.* **1996**, *118*, 11225.
[82] M. Yang, C. Liu, Z. Li, G. Gao, F. Liu, *Macromolecules* **2010**, *43*, 10645.
[83] F. Römer, A. Lervik, F. Bresme, *J. Chem. Phys.* **2012**, *137*, 074503.
[84] T. W. Sirk, S. Moore, E. F. Brown, *J. Chem. Phys.* **2013**, *138*, 064505.
[85] J. L. F. Abascal, C. Vega, *J. Chem. Phys.* **2005**, *123*, 234505.
[86] A. Glättli, X. Daura, W. F. V. Gunsteren, *J. Chem. Phys.* **2002**, *116*, 9811.
[87] T. Zhang, A. R. Gans-Forrest, E. Lee, X. Zhang, C. Qu, Y. Pang, F. Sun, T. Luo, *ACS Appl. Mater. Interfaces* **2016**, *8*, 33326.
[88] E. Espinosa, E. Molins, C. Lecomte, *Chem. Phys. Lett.* **1998**, *285*, 170.
[89] L. Zhang, M. Ruesch, X. Zhang, Z. Bai, L. Liu, *RSC Adv.* **2015**, *5*, 87981.
[90] L. Zhang, Z. Bai, L. Liu, *Adv. Mater. Interfaces* **2016**, *3*, 1600211.
[91] A. K. Soper, M. G. Phillips, *Chem. Phys.* **1986**, *107*, 47.
[92] S. S. Jang, S.-T. Lin, T. Çağın, V. Molinero, W. A. Goddard, *J. Phys. Chem. B* **2005**, *109*, 10154.
[93] E. Brini, C. J. Fennell, M. Fernandez-Serra, B. Hribar-Lee, M. Lukšič, K. A. Dill, *Chem. Rev.* **2017**, *117*, 12385.
[94] K. Nomura, T. Kaneko, J. Bai, J. S. Francisco, K. Yasuoka, X. C. Zeng, *Proc. Natl. Acad. Sci.* **2017**, *114*, 4066.
[95] G. Kikugawa, T. G. Desai, P. Keblinski, T. Ohara, *J. Appl. Phys.* **2013**, *114*, 034302.
[96] M. White, G. Dorion, *J. Polym. Sci.* **1961**, *55*, 731.
[97] L. Liu, P. Li, S. A. Asher, *J. Am. Chem. Soc.* **1999**, *121*, 4040.
[98] M. Lorenzo, Z. Nicola, M. Andrea, D. G. Matteo, C. Matteo, F. M. Letizia, T. Claudia, *Chem. - Eur. J.* **2016**, *22*, 12106.
[99] N. Tanaka, S. Matsukawa, H. Kurosu, I. Ando, *Polymer* **1998**, *39*, 4703.
[100] H. Yasunaga, I. Ando, *Polym. Gels Networks* **1993**, *1*, 83.